J. Fluid Mech. (2006), *vol.* 554, *pp.* 217–235.
doi:10.1017/S0022112005007779 Printed in the United Kingdom

Large-deformation analysis of the elastic recoil of fibre layers in a Brinkman medium with application to the endothelial glycocalyx

By YUEFENG HAN[1], SHELDON WEINBAUM[1]†, JOS A. E. SPAAN[2] AND HANS VINK[2]

[1]Departments of Biomedical and Mechanical Engineering, CUNY Graduate Center and the City College of New York, New York, NY, USA

[2]Department of Medical Physics, Academic Medical Center, University of Amsterdam, 1100 De Amsterdam, The Netherlands

(Received 28 February 2005 and in revised form 1 August 2005)

There is wide interest in the role of the endothelial surface layer (ESL) in transmitting blood shear stress to the intracellular cytoskeleton of the endothelial cell. However, very little is known about the mechanical properties of the glycocalyx or the flexural rigidity of the core proteins that comprise it. Vink, Duling & Spaan (*FASEB J.*, vol. 13, 1999, p. A 11) measured the time-dependent restoration of the ESL after it had been nearly completely compressed by the passage of a white blood cell (WBC) in a tightly fitting capillary. Using this initial experiment, Weinbaum *et al.* (*Proc. Natl. Acad. Sci. USA*, vol. 100, 2003, p. 7988) predicted that the core proteins have a flexural rigidity EI of 700 pN nm^2, which is $\sim 1/20$ the measured value for an actin filament. However, their analysis assumes small deflections and only the fibre motion is considered. In the present paper we report additional experiments and apply large-deformation theory for 'elastica' to describe the restoration of the fibres in a Brinkman medium which absorbs fluid as the ESL expands. We find that there are two phases in the fibre recoil: an initial phase for large compressions where the ESL thickness is < 0.36 its undisturbed thickness, and the ends of the fibres overlap and are parallel to the capillary wall; and a second phase where the fibres assume a shape that is close to the solutions for an elastic bar with linearly distributed vertical loading. The predicted time-dependent change in thickness of the ESL provides remarkably good agreement with experiment and yields an estimate of 490 pN nm^2 for the flexural rigidity EI of the core protein fibres, which is unexpectedly close to that predicted by the linear theory in Weinbaum *et al.* (2003).

1. Introduction

The problem of the elastohydrodynamic recoil of a matted layer of initially uniform vertical fibres in a viscous fluid arises in many contexts from the stroking of fur and the motion of the bristles of a soft brush, to the recoil of the endothelial glycocalyx after the passage of a white blood cell (WBC) in a tightly fitting capillary, the motivation for the present study. The motion of a periodic array of vertical fibres in

† Author to whom correspondence should be addressed: Department of Biomedical Engineering, The City College of New York, 138th Street at Convent Avenue, New York, NY 10031, USA weinbaum@ccny.cuny.edu

a plane wall has been studied in a variety of biological applications. Some prominent applications include beating cilia (Liron & Shahar 1978), the flow past brush border microvilli in the proximal tubule (Guo, Weinstein & Weinbaum 2000), cilia in the cortical collecting duct (Liu *et al.* 2003), and the transmission of fluid shear stress by core proteins comprising the glycocalyx that forms the endothelial surface layer (ESL) (Secomb, Hsu & Pries 2001*a*; Weinbaum *et al.* 2003). Beating cilia in a channel have been treated using Liron's extension (Liron & Mochon 1976; Liron & Shahar 1978) of Blake's singularity (Blake 1971) for the motion of a Stokeslet near a planar boundary. Since beating cilia is an active process in which the motion is prescribed, one does not need to consider their passive elastohydrodynamic response. In contrast, in problems involving mechanotransduction, such as the flow past brush border microvilli, or primary cilia in the cortical collecting duct, or core proteins in the ESL, the deformation of these cellular protuberances or molecular fibres plays a critical role since it is related to the deformation of the intracellular cytoskeleton and, hence, intracellular signalling.

The fluid flow in the three mechanotransduction problems mentioned above has been examined using effective-medium theory (Brinkman equation) and the deformations determined using a theory for the small deflections of a cantilever beam (Gere & Timoshenko 1990). These latter analyses employ the solutions of Sangani & Acrivos (1982) for the local Stokes flow past a two-dimensional hexagonal array of circular cylinders to first determine the local hydrodynamic loading on the protuberances or fibres and then use this loading to determine their deflection. There is no motion of the fibres in these analyses since the external flow is steady and the deformation is constant. These steady flow analyses were recently extended to treat the elastohydrodynamic response of the fibres in a time-dependent oscillating flow where the relative motion of the fibres and the fluid is considered (Han, Ganatos & Weinbaum 2005). This theory was limited to small fibre deformations.

A problem that has attracted widespread attention is the role of the ESL in transmitting fluid shear stress due to the flowing blood to the intracellular cytoskeleton of the endothelial cell. This problem raises a fundamental paradox since it is generally agreed that the flow within the ESL is negligible and the shear stress at the level of the cell membrane vanishingly small (Damiano 1998; Feng & Weinbaum 2000; Secomb, Hsu & Pries 1998; Secomb, Hsu & Pries 2001*b*; Weinbaum *et al.* 2003). Various models have been proposed to explain the mechanism via which the shear stress is transmitted to either the cell membrane or the cell's actin cytoskeleton and why the ESL maintains its structural rigidity under flow (Damiano & Stace 2002; Secomb *et al.* 2001*a*, *b*; Weinbaum, *et al.* 2003). Secomb *et al.* (2001*a*, *b*) propose that its structural integrity arises from an oncotic force due to trapped plasma proteins. Damiano & Stace (2002) suggest that this is due to electrochemical effects associated with the negative charge on the glycosaminoglycans (GAG) of the glycocalyx. Weinbaum *et al.* (2003) propose that it arises from the flexural rigidity EI of the core proteins of the ESL. The merits and deficiencies of each model are summarized at the end of the paper.

While the existence of the ESL and the first measurements of its thickness *in vivo* were obtained in Vink & Duling (1996), the three-dimensional structural organization of the ESL was not realized till Squire *et al.* (2001) were able to identify for the first time the quasi-periodic substructure of the glycocalyx and its anchoring foci. The latter appear to emanate from the underlying actin cortical scaffold beneath the membrane which takes the form of an ordered hexagonal array. The model proposed in Squire *et al.* (2001) was developed into an idealized mathematical model in Weinbaum

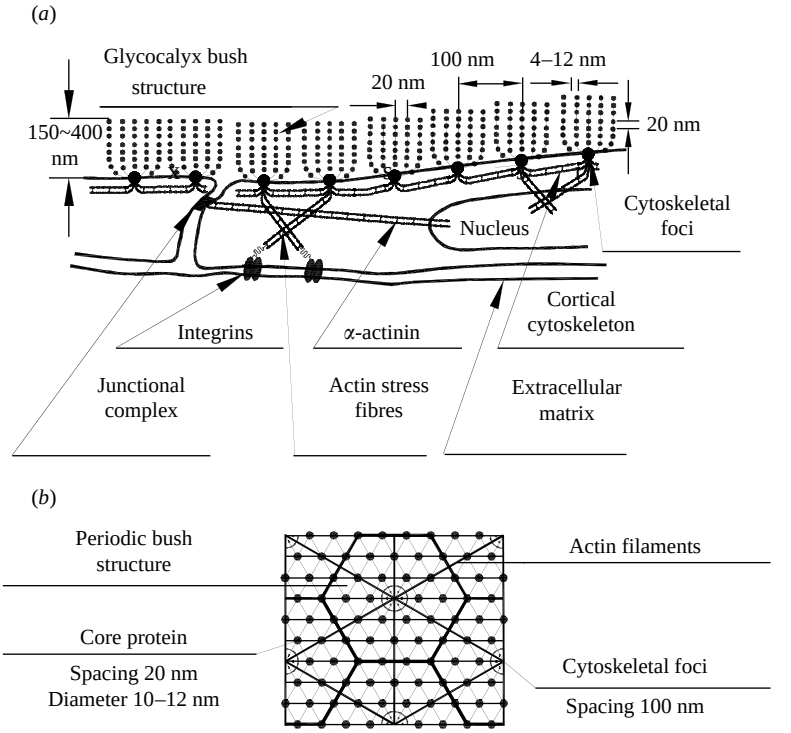

FIGURE 1. Structural model for the endothelial surface layer (ESL) from Squire *et al.* (2001) and Weinbaum *et al.* (2003). (*a*) Sketch of the arrangement of core proteins in the ESL and its anchorage to the underlying cortical cytoskeleton. (*b*) *En face* view of the structural model showing the hexagonal arrangement of core proteins and cluster foci.

et al. (2003). This idealized model with its characteristic dimensions is shown in figure 1. The basic structural elements of the ESL are assumed to be the core proteins of proteoglycans, the most likely candidate being syndecan I, a transmembrane heparin sulphate proteoglycan (Mulivor & Lipowsky 2004). Hyaluronan and chondroitin sulphate also play an important role in its assembly and sieving properties (Henry & Duling 2000). Recent studies have shown that the primary functions of the ESL are not only to protect the endothelium, but also to serve as a mechanotransducer of fluid shear (Weinbaum *et al.* 2003; Thi *et al.* 2004) and a molecular sieve for plasma proteins (Michel 1997; Weinbaum 1998; Hu *et al.* 2000; Adamson *et al.* 2004). A review of the state of knowledge of the ESL, its properties and function is given in Pries, Secomb & Gaehtgens (2000).

Very little is known about the mechanical properties of the glycocalyx or the flexural rigidity, EI, of the core proteins that comprise it. However, Vink, Duling & Spaan (1999) reported an initial experiment from which these properties can be deduced with the aid of a mathematical model. This experiment, which was published as an abstract, is described in detail in the present study. In the experiment one measures the time-dependent restoration of the ESL after it is nearly completely compressed by the passage of a WBC in a tightly fitting capillary. This restoration is estimated by measuring the gap between the endothelial cell (EC) membrane and the membranes of red blood cells (RBCs) that follow at different distances in the wake of the WBC. One finds that the characteristic time for the restoration is approximately

0.4 s. Damiano & Stace (2002) and Weinbaum *et al.* (2003) have both attempted to predict this characteristic time using either an electrochemical or elastic mechanism for the recoil of the crushed ESL. The elastic model in Weinbaum *et al.* (2003), which is the catalyst for the present study, predicts that two characteristic times describe the recoil: a short time associated with the relaxation of the initial shape of the core proteins after their compression, and a long-time behaviour associated with the final phase of the motion. EI is determined by requiring that the latter time match the measured value 0.4 s taken for the ESL to return to its initial undisturbed thickness. Using a time-dependent beam equation for small deflections, in which the local force on the fibre is proportional to its local instantaneous velocity, it was predicted that the core proteins have a flexural rigidity EI of $700\,\mathrm{pN\,nm^2}$. This is about 1/20 the measured value for an actin filament, the structural element beneath the membrane that anchors the bush-like core protein structure, see figure 1.

The foregoing linear analysis in Weinbaum *et al.* (2003) was intended only as a rough guide for predicting EI. The large initial deformations of the core proteins lie far outside the range of validity of the small-deflection theory used in their analysis and the fibres were assumed to recoil in a stagnant fluid. No attempt was made to predict the time-dependent change in shape of the fibres during their recoil. Furthermore, the analysis in Han *et al.* (2005) shows that the motion of the fibres induces a motion of comparable magnitude in the fluid in planes parallel to the membrane and the latter was neglected in Weinbaum *et al.* (2003). In the present paper a more sophisticated nonlinear analysis is attempted which is a more realistic representation of the mechanics of the fluid and fibre motion. Large-deformation theory for 'elastica' is applied to describe the time-dependent motion of the fibres and their changing shape. In addition, the fluid flows in directions both normal and parallel to the wall are considered. The flow normal to the wall is of special interest since the displaced volume occupied by the fibres induces a normal velocity that entrains fluid into the fibre layer as the fibres recoil and the solid fraction decreases. The flow in the direction parallel to the wall is very similar to the analysis in Han *et al.* (2005). There is very little relative motion of fluid and fibre in this direction except for a thin fibre interaction layer near the edge of the glycocalyx. Two phases are found in the fibre recoil: an initial phase for large compressions where the glycocalyx thickness is < 0.36 of its uncompressed state and the ends of the fibres overlap and a second phase where the fibres assume a shape that is very similar to the well-known solutions for an 'elastica' with a linearly varying load. Using this model for large deformation, we also predict the time-dependent change in shape of the glycocalyx fibres during the recovery of the ESL.

The body of the paper will be divided into four sections: a methods and results section describing the experiments for the glycocalyx recoil, a theoretical section describing the formulation and solution of the nonlinear large-deformation equations for the time-dependent change in the shape of the fibres, a results section comparing theory and experiment and a discussion section which will explore the plausibility of various mechanisms that have been proposed for the glycocalyx recoil.

2. Experimental methods and results

2.1. *Methods*

The cremaster muscle of hamsters was prepared as in described Constantinescu, Vink & Spaan (2000). The cremaster muscle was observed with an intravital microscope (Olympus BHM) and a cooled ICCD video camera (GenIV ICCD,

Princeton Instruments). The tissue was transilluminated with a Hg lamp (100 W) equipped with a 435 nm bandpass interference filter (blue light) using an aplanat (lens free from spherical aberration), achromatic condenser set at numerical aperture (NA) 1.2 (U-AAC, Olympus). All preparations were examined with a ×60 water immersion objective lens (Olympus, UPlanApo NA 1.2 W or LUMPlanFL NA 0.9 W) and a telescopic tube to give a final object-to-camera magnification of ×200. Images were displayed on a Philips CM 8833-II video monitor and recorded using a SVHS video tape recorder (JVC BR-S611E) and a time coding interface unit (JVC SA-F911E) for further image analysis.

Video images were digitized using a frame grabber (DT3152, PCI Local Bus) and Image-Pro Plus software (Image-Pro Plus version 3.0, Media Cybernetics, Silver Spring, PA, USA). An onscreen caliper using a 1 mm/0.01 mm stage micrometer was used for all calibrated dimensional measurements. The anatomical capillary diameter and the width of the flowing red blood cell column were measured using digital calipers at the inside of the capillary wall to determine the dimension of the endothelial–RBC gap prior to, during and after spontaneous capillary leukocyte passage.

2.2. *Results*

A microscopic image of a transilluminated hamster cremaster muscle capillary is shown in figure 2(*a*). The gap between the membranes of flowing RBCs and ECs is clearly identified, being greater in larger capillaries as previously shown (figure 2(*b*), from Vink *et al.* 1999). The dimensions of RBC–EC gaps in small ($D = 4.2 \pm 0.1\,\mu$m, $n = 21$), medium ($D = 5.1 \pm 0.0\,\mu$m, $n = 82$) and large ($D = 6.2 \pm 0.1\,\mu$m, $n = 94$) capillaries are 0.3 ± 0.03, 0.5 ± 0.02 and $0.7 \pm 0.04\,\mu$m respectively. Figures 3(*a–d*) shows the results of four experiments describing the recovery of the RBC–EC gap after the passage of a WBC in capillaries varying from 4.4 to 6.0 μm diameter. Layer recovery times (t) after WBC compression range between 0.5 and 1.0 s and correlate with capillary diameter (D): $t = 0.26D - 0.62$ ($n = 6$, $P < 0.05$), i.e. recovery times are shorter in smaller capillaries. Consequently, layer recovery rates are, surprisingly, independent of capillary diameter: RBC–EC gap dimension/t is 0.64 ± 0.06, 0.71 ± 0.03 and $0.71 \pm 0.04\,\mu\text{m s}^{-1}$ ($P = NS$) in small, medium and large capillaries (figure 2*c*, from Vink *et al.* 1999). Figure 3(*a–d*) shows a nonlinear restoration of the glycocalyx layer that ends rather quickly when the initial layer thickness is approached. There is no long-time asymptotic behaviour. It is this essential feature that our non-linear model will attempt to replicate. The characteristic rise time for full restoration varies from 0.5 to 1.0 s. The experiment which provided the largest compression of the ESL and the most detailed set of data is for the 4.4 μm capillary shown in figure 3(*a*). In this experiment we estimated the ESL was crushed to 20 % to 25 % percent of its initial undisturbed thickness. Such large fibre deformations fall far outside the range of cantilever beam theory and are described more accurately by 'elastica' theory.

3. Mathematical model

RBCs produce a slow draining of the ESL when brought to rest, with a characteristic draining time of 0.5 s (Weinbaum *et al.* 2003), and gradually rise through the ESL as their velocity increases when flow is started again. In contrast, WBCs are much stiffer, in view of their nuclei and cytoskeletal organelles and, as observed in figure 3, the initial compression of the ESL by the passing WBC is nearly instantaneous and independent of its velocity. The mechano-electrochemical model in Damiano & Stace (2002) and the elastic recoil model in Weinbaum *et al.* (2003) were largely

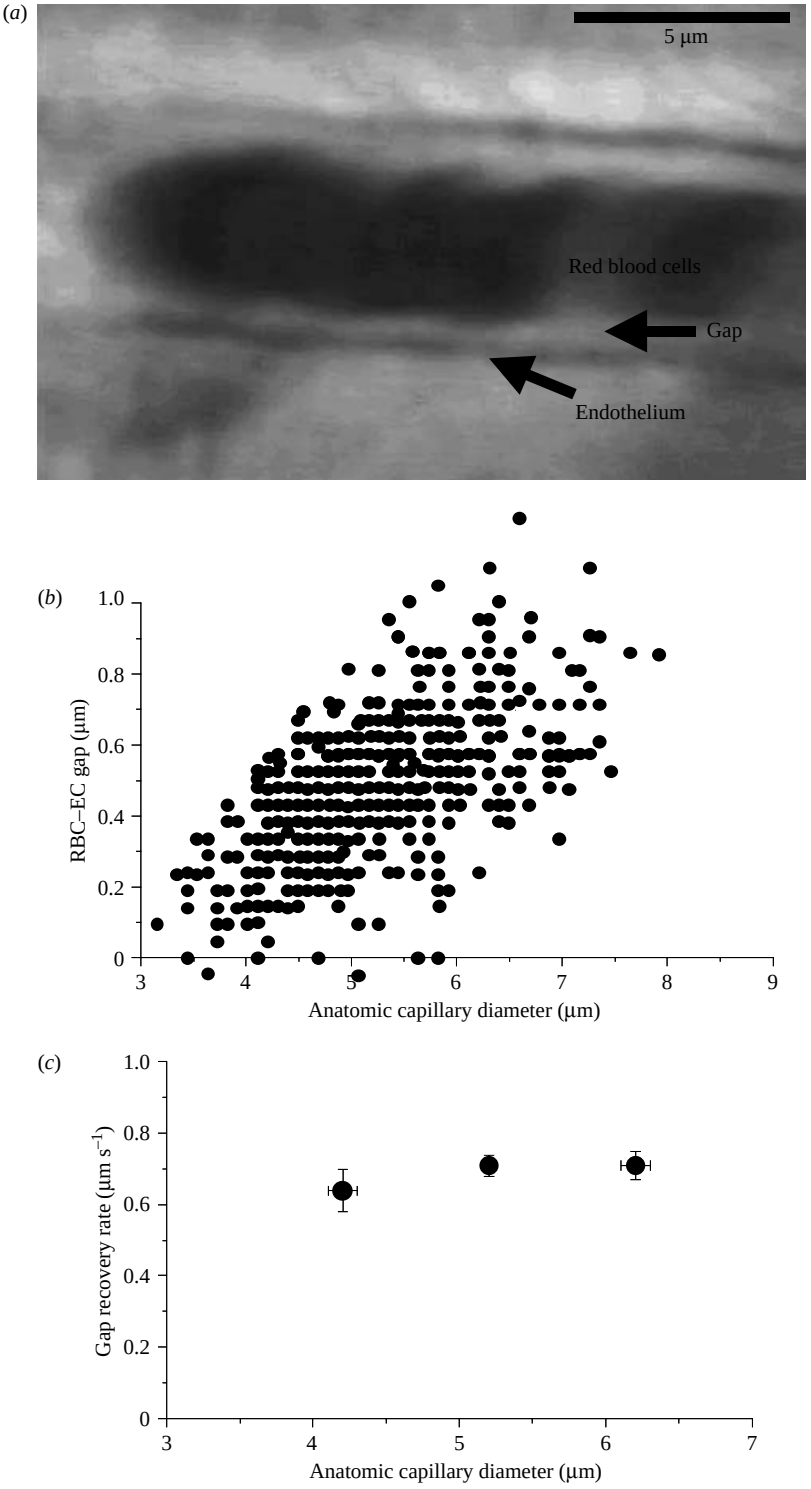

FIGURE 2. (*a*) Microscopic image of a transilluminated hamster muscle capillary showing the measurement of RBC–EC gaps; (*b*) the relation between anatomic capillary diameter and RBC–EC gap size; and (*c*) the gap recovery rate as a function of capillary diameter.

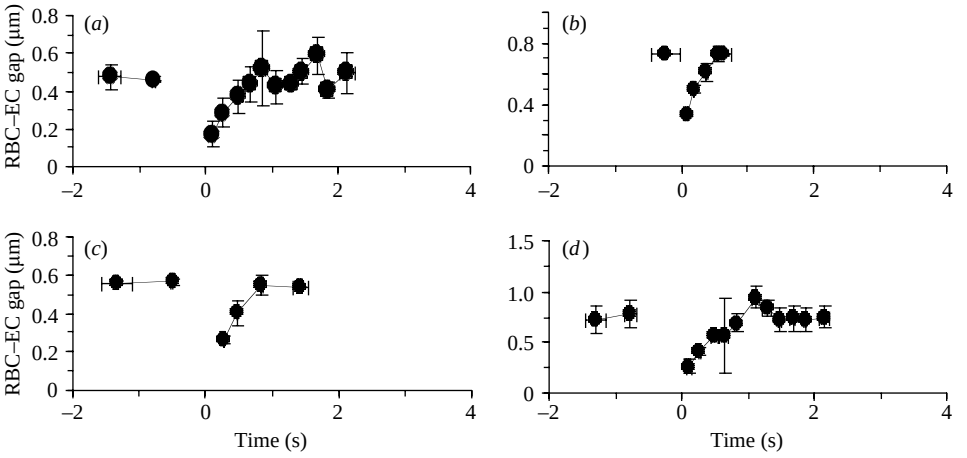

FIGURE 3. RBC–EC gap recovery as a function of time after the passage of a WBC through a capillary with a diameter of (*a*) 4.4 μm, (*b*) 5.1 μm, (*c*) 5.2 μm, and (*d*) 6.0 μm.

concerned with predicting the characteristic time for this restoration and not the detailed time-dependent change in the shape of the fibres during their recoil. It is also clear from the observed structure of the ESL (Squire *et al.* 2001), and the size of the scattering centres along the core proteins depicted in figure 1, that the volume fraction of the solid matrix could approach near close packing for the very large deformations observed in figure 3(*a*). These observations suggest that a realistic model needs to include both the changing solid fraction c of the expanding glycocalyx and realistic shapes of the core proteins from the initial passage of the WBC till the final restoration of the ESL. Thus, the formulation of the theoretical model is divided into two major subsections: a model for the fluid flow and a model for the instantaneous fibre or core protein shape. The fluid flow model must take account of both the instantaneous x and y components of the velocity of the fluid and the recoiling core proteins and the changing solid fraction, the latter at least in a time-average sense. This changing value of c provides a source term for entraining fluid and, thus, adds to the drag on the fibres. The fibre model exploits a realistic family of shapes obtained from known solutions to the 'elastica' equations and simple experiments where the qualitative shape of an 'elastica' is observed when a flat planar surface moves over the fibre.

3.1. *Model for the fluid*

The fluid flow in the recoiling fibre layer is modelled as a flow in a porous medium with an average time-dependent solid fraction c, as shown in figure 4. Physiologically, there is a pressure gradient in the x-direction. However, the velocity it generates is $<10\,\mathrm{nm\,s^{-1}}$ in the interior of the ESL for the fibre geometry depicted in figure 1, and thus negligible compared to the fibre recoil velocity. Furthermore, the fluid flow varies slowly in the x-direction. Thus, we will neglect the pressure gradient in the x-direction and the first and second derivatives of the fluid velocities with respect to x in the continuity equation and the Brinkman equation describing the fluid fibre momentum balance. The continuity equation contains a source term with a time-varying solid fraction,

$$\frac{\partial(1-c)}{\partial t} + \frac{\partial u_y}{\partial y} = 0. \tag{1}$$

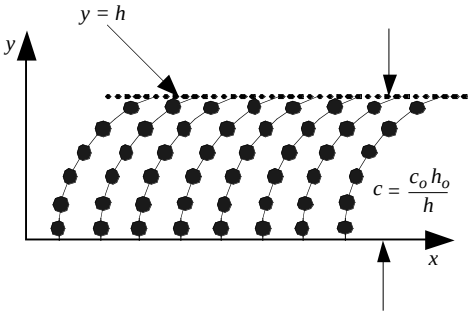

FIGURE 4. Simplified model for the structure of the ESL. The ESL is modelled as a porous medium with an average solid fraction c dependent on the ESL thickness, with scattering centres (black dots) 12 nm diameter located at 20 nm intervals along axes of the core proteins.

Here u_y is the fluid velocity component in the y-direction and c is the instantaneous average solid fraction of the ESL. The uncompressed ESL has a solid fraction of 0.16 using a structural model with 12 nm diameter spherical scattering centres spaced at 20 nm intervals along the axes of the core proteins as shown in figure 1. The inertia of the fluid is negligible. The governing Brinkman equations for the fluid motion, which take account of the quasi-steady relative motion of the fluid and the fibres in the x- and y-directions, are

$$u_x - \frac{\partial v_x}{\partial t} = K_{Px}\frac{\partial^2 u_x}{\partial y^2}, \tag{2}$$

and

$$\frac{\partial P}{\partial y} = \mu\frac{\partial^2 u_y}{\partial y^2} - \frac{\mu}{K_{Py}}\left(u_y + \frac{\partial v_y}{\partial t}\right). \tag{3}$$

Here P is the fluid pressure, μ is the fluid viscosity, K_{Px} and K_{Py} are Darcy's permeability of the ESL in the x- and y-directions, respectively, and v_x and v_y are the fibre deflections in the positive x and negative y directions, respectively, and are functions of x, y and t. The applicability of using a Brinkman equation to describe the fluid motion in the ESL is described at length in Damiano *et al.* (1996) and Feng, Ganatos & Weinbaum (1998). Despite its limitation in describing the transition from a Darcy flow in the interior of the ESL to a steady laminar flow outside this layer, it has been used in nearly all recent theoretical studies for the fluid flow in this layer. As we shall show shortly, the transition layer is of little importance in the present study and the viscous term can be dropped.

The solid mass is conserved throughout the fibre recoil process. Thus,

$$c = \frac{c_o h_o}{h}, \tag{4}$$

where h is the instantaneous ESL thickness, and c_o and h_o are the uncompressed solid fraction and thickness. Note that (4) neglects the local variation of c as a function of y. The instantaneous solid fraction, c, is treated as an average value for the entire ESL that satisfies the global mass balance for the layer. This approximation greatly simplifies the analysis. Combining (1) and (4), one obtains

$$u_y = y\frac{\mathrm{d}c}{\mathrm{d}t} = -\frac{y c_o h_o}{h^2}\frac{\mathrm{d}h}{\mathrm{d}t}. \tag{5}$$

Let us assume that the characteristic length l_c is the uncompressed ESL thickness h_o, 400 nm, and the characteristic velocity in the x-direction for both the fluid and the fibre tip is the fluid velocity at the ESL edge. Thus, the term, $K_{Px}\partial^2 u_x/\partial y^2$, in (2) has a scale of K_{Px}/l_c^2, $\sim 10^{-4}$ since the Darcy's permeability, K_{Px}, of the undeformed ESL is 3.16 nm^2 (Han *et al.* 2005; Weinbaum *et al.* 2003). Thus, equation (2) can be rewritten as

$$u_x = \frac{\partial v_x}{\partial t} \tag{6}$$

except for a thin tip interaction layer at the edge of the ESL where the higher-order derivative term $K_{Px}\partial^2 u_x/\partial y^2$ is required to describe the flow transition at the ESL edge. The solutions in Han *et al.* (2005) and Weinbaum *et al.* (2003) show that this slip velocity is typically a few $\mu m\,s^{-1}$ when the fluid shear stress at the ESL edge is $10\,dyn\,cm^{-2}$. In the present application this shear stress is much smaller due to the slow velocity of the WBC. In the interior of the fibre layer the fluid flow induced by the edge velocity is negligible. In contrast, the fluid flow induced by the fibre motion is dominant. Thus, equation (6) is a good approximation except for the tip interaction boundary layer at the outer edge of the ESL which is described in Guo *et al.* (2000) and Han *et al.* (2005). Substituting (5) into (3), one obtains

$$\frac{\partial P}{\partial y} = \frac{\mu}{K_{Py}}\left(\frac{\partial v_y}{\partial t} - \frac{y c_o h_o}{h^2}\frac{\mathrm{d}h}{\mathrm{d}t}\right). \tag{7}$$

Equations (5)–(7) define the fluid velocity and pressure field except for the tip interaction layer. Both fields depend on the instantaneous ESL thickness $h(t)$, its velocity $\mathrm{d}h/\mathrm{d}t$ and the local components of the fibre velocity, $\partial v_x/\partial t$ and $\partial v_y/\partial t$.

3.2. *Time-dependent fibre recoil*

Figure 5 shows our two-phase fibre recoil model schematically. As alluded to earlier, the qualitative shape of a deformed fibre after the passage of a WBC can be deduced from simple experiments in which a planar boundary is passed at different heights over a thin vertical elastic strip rigidly anchored at its base. One finds that the strip takes the shape of an 'elastica' that is loaded at its tip until the point of contact with the planar boundary and that from there to its end the strip is parallel to the planar surface. This is the initial assumed shape of the fibres after the passage of the WBC. In phase I it is assumed that the fibres recoil through a family of shapes which have this basic geometry with the location of the zero-slope point shifting towards the end of the fibre as it rises (dashed line $\mathrm{d}v_y/\mathrm{d}x = 0$ in figure 5). With closely spaced fibres that overlap near their top surface this geometry is quite realistic. At the transition point at the end of phase I ($h = h_t$), the slope of the fibre at its tip is horizontal. In phase II, the slope at the fibre tip continues to increase as the fibre recoils back to its original upright shape from the transition point.

3.2.1. *Hydrodynamic loads on the core protein fibre*

The fluid drag force on the core protein fibre is proportional to the relative velocity between the fluid and the fibres. However, equation (6) shows that there is no relative velocity in the x-direction except in the tip boundary layer, which we neglect. Furthermore, the solutions in Han *et al.* (2005) and Weinbaum *et al.* (2003) show that the fluid shear stress at the ESL edge causes a very small deflection of the core protein fibres compared to the large deformation caused by the passage of the WBC in the present analysis. This small deflection describes the final steady state after the fibre recoil is completed. In contrast, there is a substantial relative velocity in the

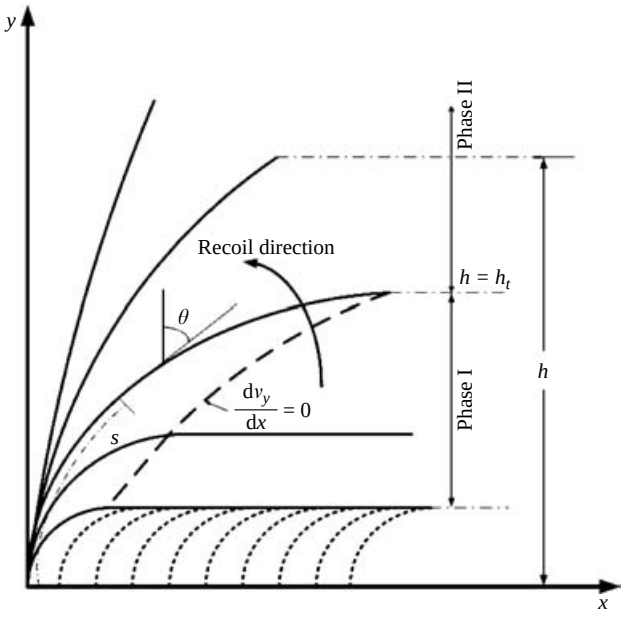

FIGURE 5. Parametric family of shapes for core protein fibres during the ESL recovery. In phase I the tip ends of core protein fibres are matted and in phase II the core protein fibres are no longer matted and have a slope >0 at their ends.

y-direction between the fluid and fibres due to the entraining effect of the recoiling fibre layer and the fact that the fibre is moving upward relative to the fluid whose normal velocity vanishes at $y=0$. The relative motion of the fluid and the fibres is, therefore, much greater in the y-direction than in the x-direction and the latter can be neglected. We decompose the drag force due to the relative motion in the y-direction into force components normal, n, and tangent, t, to the local fibre direction since the drag coefficients or the Darcy permeability differ for flow normal and tangent to the fibres. We write the drag force in vector form as

$$\boldsymbol{f} = \{f_n, f_t\} = \mu \frac{\pi}{c} r^2 \left(u_y + \frac{\partial v_y}{\partial t} \right) \left\{ \frac{\cos\theta}{K_{Pn}}, \frac{\sin\theta}{K_{Pt}} \right\}. \tag{8}$$

Here θ is the local tangent angle of the fibre and K_{Pn}, K_{Pt} are the Darcy permeability for the flow normal and tangent to the fibre, respectively. Substituting (5) into (8), one obtains

$$\boldsymbol{f} = \{f_n, f_t\} = -\mu \frac{\pi}{c} r^2 \left(\frac{y c_o h_o}{h^2} \frac{\mathrm{d}h}{\mathrm{d}t} - \frac{\partial v_y}{\partial t} \right) \left\{ \frac{\cos\theta}{K_{Pn}}, \frac{\sin\theta}{K_{Pt}} \right\} \tag{9}$$

where r is the fibre radius. In (9) we compute the local drag force by modelling the bead–fibre structure of the core proteins in figure 1 as a uniform fibre whose radius is that of the bead to simplify the analysis. As shown earlier, in phase I ($h < h_t$) the ends of the fibres overlap and form a thin layer where portions of the fibre ends are in contact with one another. The viscous resistance of this overlapping region is balanced by the elastic restoring force at the initial contact points of the fibres with the underside of the layer, as shown by the dotted lines in figure 5. Thus, the flat portions of the fibres move upward but remain horizontal and parallel to the

capillary wall during phase I. The flat portion of a fibre exerts no restoring force since no bending energy is stored in a region of no curvature.

The instantaneous shape of core protein fibres subject to the distributed load given by (9) satisfies an 'elastica' equation for the large deformation of an elastic strip. The governing equation in θ, s intrinsic coordinates is given by (Frisch-Fay 1962):

$$EI\frac{\partial\theta}{\partial s} = \int_s^{h_o}\left[(f_n(\xi,t)\cos(\theta) + f_t(\xi,t)\sin(\theta))\int_s^{\xi}\sin(\theta)\,\mathrm{d}\zeta + (f_n(\xi,t)\sin(\theta) - f_t(\xi,t)\cos(\theta))\int_s^{\xi}\cos(\theta)\,\mathrm{d}\zeta\right]\mathrm{d}\xi. \tag{10}$$

Here EI is the flexural rigidity of core protein fibres, $f_n(\xi,t)$ and $f_t(\xi,t)$ are normal and tangential components of the local instantaneous load and ξ, ζ are dummy variables. The integro-differential equation (10) cannot be solved in a closed form, except for the special case of a concentrated vertical load applied at the fibre tip (Frisch-Fay 1962). Numerical solutions are also available for a uniform or linearly varying load (Lee, Wilson & Oh 1993). In the current application, the numerical procedures in ANSYS (v8.0, commercially available from ANSYS, Inc.) are used to solve (10) for an arbitrary $\boldsymbol{f}(\xi,t)$.

3.2.2. *Non-dimensionalization*

It is convenient to introduce the following dimensionless variables and parameters:

$$h^* = \frac{h}{h_o}, \quad y^* = \frac{y}{h_o}, \quad v_y^* = \frac{v_y}{h_o} \quad t^* = \frac{t}{\tau}, \quad \boldsymbol{f}^* = \frac{\boldsymbol{f}h_o^3}{EI}. \tag{11}$$

Here τ is the dimensional reference time, which is defined as

$$\tau = \frac{\pi}{c_o}\frac{r^2}{K_{pn}}\frac{\mu h_o^4}{EI}. \tag{12}$$

Equation (9) can be rewritten in dimensionless form as

$$\boldsymbol{f}^* = -\frac{c_o}{c}\left(\frac{c_o y^*}{h^{*2}}\frac{\mathrm{d}h^*}{\mathrm{d}t^*} - \frac{\mathrm{d}v_y^*}{\mathrm{d}t^*}\right)\{\cos\theta,\, K_r\sin\theta\}. \tag{13}$$

Here $K_r = K_{Pn}/K_{Pt}$. One can obtain the distributed hydrodynamic load along the fibre from (13) if the fibre shape and the local small displacements, $\mathrm{d}h^*$ and $\mathrm{d}v_y^*$, in the time interval $\mathrm{d}t^*$ are known. Equations (10) and (13) can be solved numerically at each time step by an iteration procedure as described next.

3.2.3. *Numerical solution procedure*

(i) Starting from a prescribed fibre shape whose tip height is h^* at time t^*, one guesses a new fibre shape whose tip height is $h^* + \mathrm{d}h^*$ and as an initial guess assumes other points are displaced by an amount $\mathrm{d}v_y^*$ which increases linearly with distance along the fibre subject to $\mathrm{d}v_y^* = \mathrm{d}h^*$ at $s^* = 1$ at time $t^* + \mathrm{d}t^*$. (ii) One then computes the hydrodynamic load using (13) for the assumed value of $\mathrm{d}h^*$ and the guessed displacement distribution $\mathrm{d}v_y^*$. The assumed time interval $\mathrm{d}t^*$ serves as a scaling constant for the loading $\boldsymbol{f}^*$. (iii) Using the loading from step (ii), one calculates the fibre shape from (10) and the upward displacement of the fibre tip $\mathrm{d}h^*$ using the numerical program for the 'elastica' in ANSYS. The value of $\mathrm{d}t^*$ is set by requiring that the assumed $\mathrm{d}h^*$ and the predicted $\mathrm{d}h^*$ from the ANSYS program agree. This completes the first iteration. (iv) One now uses this newly computed shape to provide

new values for dv_y^* and $dh^*$and iterates steps ii–iv until the new fibre shape converges. The criterion for convergence is that the integral $\int_{s^*=0}^{s^*=1} |v_y^{*n} - v_y^{*n-1}| ds^* < 0.001$ where v_y^{*n-1} and v_y^{*n} denote the vertical deflection of the same fibre element at the $n-1$ and n iteration. Since the shape of the fibre is not very sensitive to the detailed loading, one can achieve convergence after less than 10 iterations. (v) This new shape at $t^* + dt^*$ is then treated as a known shape and steps (i–vi) are repeated until the fibre layer is fully restored. In this manner, one obtains the fibre layer dimensionless height h/h_o, the dimensionless fibre deflection v_x/h_o, v_y/h_o and the dimensionless fibre loading $\boldsymbol{f} h_o^3/EI$ as a function of t/τ.

Figures 7(*b*) and 7(*c*) below show that the normal hydrodynamic load on the fibre increases monotonically with distance s along the fibre length and the tangential load has a complex distribution which changes shape in passing from phase I to phase II. At the transition between phase I and II, the dimensionless transition height of the fibre layer, $h_t^* = h_t/h_o$, would be 0.367 for a linearly varying vertical load. In phase I ($h^* < h_t^*$) the curved portion of the fibre is similar to the fibre shape at $h^* = h_t^*$ except that the fibre behaves as if it has a foreshortened length l in this region. Thus, the horizontal portion carrying no net load is $h_o - l$. The initial fibre shape for phase I is assumed to be that of a fibre subject to a linearly varying load on its curved portion plus its horizontal end segment. The initial height of this flat segment is the measured initial thickness of the ESL in the experiment. The initial fibre shape for phase II is the fibre shape at the end of phase I.

4. Results

Figure 6 compares our theoretical prediction for h/h_o with the experimental data in figure 3(*a*) and also shows the predictions derived from the data in figure 2(*b*) of Damiano & Stace (2002). In the experiment, we measured the gap between the RBC membrane and the EC membrane. This gap includes two layers: the ESL and a lubricating plasma layer between the RBC membrane and the ESL surface (Secomb *et al.* 2001; Vink & Duling 1996; Weinbaum *et al.* 2003). The measured velocity of the WBC and hence the velocity of the trailing RBCs in figure 3(*a*) is approximately $50\,\mu\mathrm{m\,s^{-1}}$. At this velocity the results in figure 3 of Vink & Duling (1996) indicate a plasma layer thickness of approximately 70 nm. If we subtract this estimated plasma layer thickness from the measured gap of 470 nm between the RBC and EC cell membranes before the passage of the WBC we estimate that the undisturbed ESL thickness is 400 nm. In figure 6, the measured ESL thickness is normalized by its undisturbed thickness, 400 nm, and the experimental time is normalized by the dimensional reference time τ in (12). An optimum fit between theory and experiment is obtained for $\tau = 14$ s. All the parameters in (12) are either measured or can be theoretically approximated except the flexural rigidity EI. K_{Pn} and K_{Pn} are estimated using formulae for the flow perpendicular (Sangani & Acrivos 1982) and parallel (Cowin, Weinbaum & Zeng 1995) to a periodic array of parallel fibres. If $h_o = 400$ nm, $c_o = 0.16$, $\mu = 1.2$ cP, $r = 6$ nm, $K_{Pn} = 3.16\,\mathrm{nm^2}$ (Weinbaum *et al.* 2003) and $K_{Pt} = 6.08\,\mathrm{nm^2}$ (Sugihara-Seki 2005), one finds that $EI = 490\,\mathrm{pN\,nm^2}$. The data taken from Damiano & Stace (2002) are shifted to the right by 0.01 since the starting point in their calculation is $h/h_o = 0.5$. There are no theoretical predictions for the early large-deformation portion of the recovery. The data in Damiano & Stace (2002) are scaled by a factor of 4900 since they use a different reference time in their model.

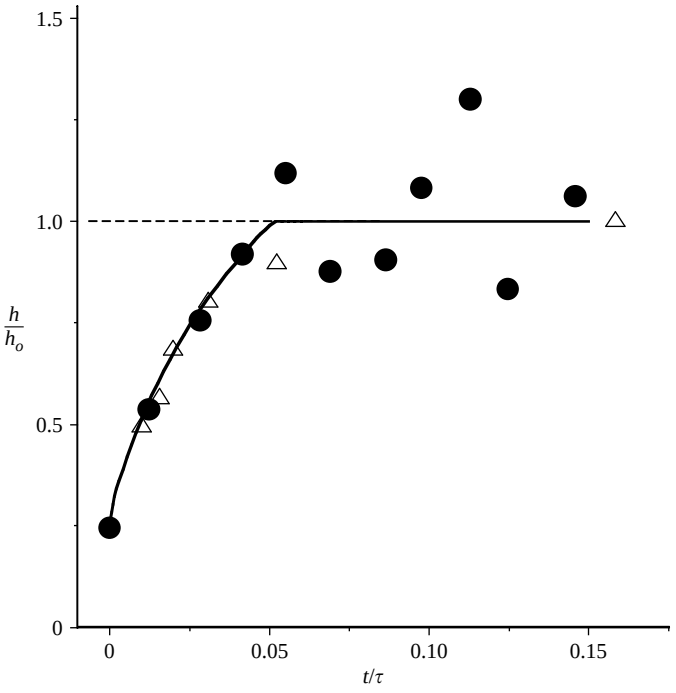

FIGURE 6. Comparison of our model predictions (solid line) and the predictions (open triangles) of figure 2(*b*) in Damiano & Stace (2002) with the experiment results shown in figure 3(*a*) (black dots). The ESL thickness is normalized by 400 nm, the undisturbed ESL thickness, and the recovery time is normalized by the dimensional reference time defined by (12) with a value of 14 s. The data taken from Damiano & Stace are rescaled by a factor of 4900 and shifted to right by 0.01 since the starting point of their recovery of the ESL is 0.5 its initial thickness.

Figure 7(*a*) shows the computed fibre shapes and figures 7(*b*) and 7(*c*) show the normal and tangential hydrodynamic loading, respectively, at different times during restoration. The transition between phase I and II occurs at 0.041 s when $h_t^* = 0.36$. The fibre shapes are not very sensitive to the detailed load distribution as long as the fibre tip is displaced to the same height. Thus, the transition height predicted herein, $h_t^* = 0.36$, is very close to the value $h_t^* = 0.367$ that would be predicted for a linearly increasing vertical load distribution.

5. Discussion

We have used effective-medium and 'elastica' theory for the large deformation of elastic fibres to model the core protein fibre recoil after compression by the passage of a WBC in a tightly fitting capillary. We estimated the flexural rigidity EI of the core protein fibres by fitting the predictions of the model to the experimental data for the time-dependent restoration of the ESL. The predicted value of EI is 490 pN nm^2, which is 70 % of the value 700 pN nm^2 predicted in Weinbaum *et al.* (2003) and about 3 % of the measured value for an actin filament (Dupuis *et al.* 1997; Gittes *et al.* 1993). This flexural rigidity of the actin filaments is required for the core proteins to be rigidly supported at their base. The present model is a major improvement of our previous model in Weinbaum *et al.* (2003) since we consider the relative motion of the fluid and fibres, use a realistic family of shapes for the fibre recoil and use

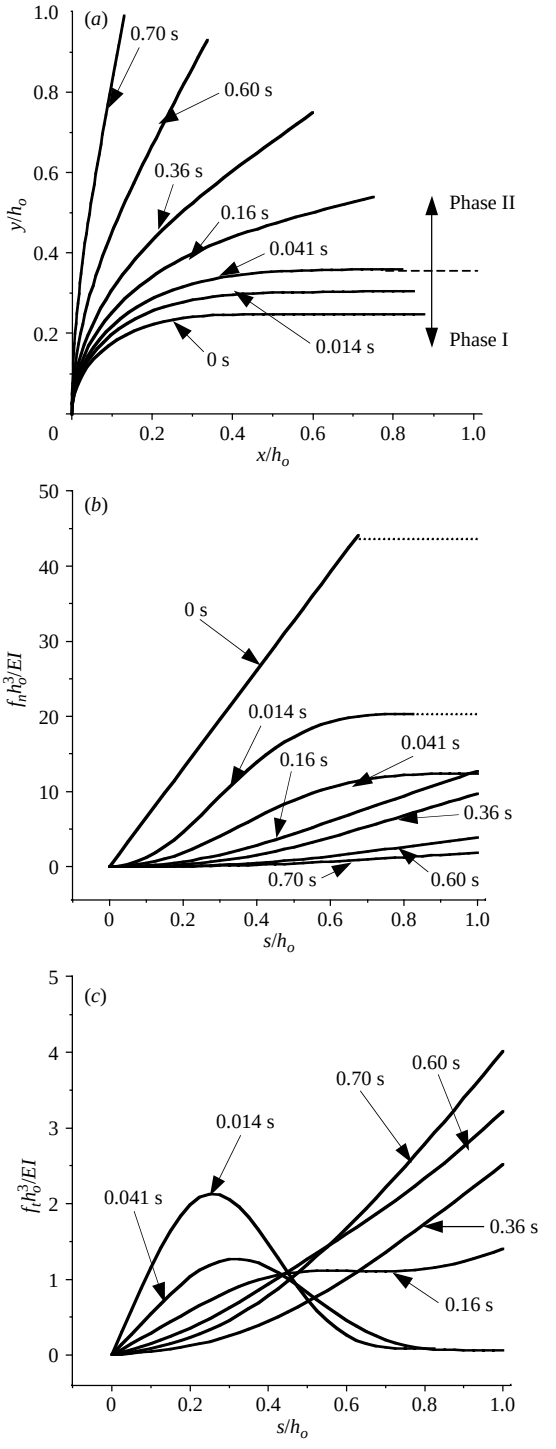

FIGURE 7(*a–c*). For caption see facing page.

large-deformation theory for 'elastica' to describe the recoil process. In contrast, Weinbaum *et al.* (2003) assumed a stagnant fluid and used small-deformation theory. Considering these improvements in the model it is rather surprising that the predicted value of EI differs by only 30 %. This is probably due to the fact that the large-deformation portion of the recoil in phase I is short lived compared to the total recoil, see figure 7(*a*).

It has long been recognized that the microvascular endothelium is covered with an ESL – a matrix layer of proteoglycans and glycoproteins. *In vivo* observations show that the ESL maintains structural integrity with little deformation when subject to the fluid shear stress of flowing blood (Vink & Duling 1996) and is restored to its original thickness after being crushed by the passage of WBCs as observed herein. These observations suggest that the layer has structural stiffness and elastic, oncotic or electrochemical restorative properties (Damiano & Stace 2002; Pries *et al.* 1997; Secomb *et al.* 2001*a*, *b*; Weinbaum *et al.* 2003).

Wiederhielm & Black (1976) found that insoluble collagen exhibits a remarkable volume exclusion effect on plasma proteins and the oncotic pressure of a plasma protein solution is increased considerably when it is mixed with collagen and hyaluronate. Thus, Pries *et al.* (1997) suggest that the colloid osmotic pressure in the endothelial glycocalyx layer may exceed that of blood plasma due to loosely adsorbed plasma proteins on the glycocalyx component even in the absence of collagen and this increase of osmotic pressure must be balanced by tension along the core protein from a mechanical point of view. In this way, an externally applied force is needed to release the tension and deform the glycocalyx layer. Experiments in Pries *et al.* (1998) show that reduction of plasma protein levels in microvessels *in vivo* lead to reduced flow resistance and they hypothesize that the glycocalyx layer becomes thinner since fewer proteins are adsorbed. Secomb *et al.* (2001*a*, *b*) argue that the difference in oncotic pressure required to maintain ESL thickness is extremely small, of the order 20 dyn cm^{-2}, and use this estimate to theoretically predict the deformation of the glycocalyx layer when RBCs pass through a capillary. This model provides reasonable predictions of the 'pop out' phenomenon, the lift off of the red cell from the capillary wall and its rise through the ESL as its velocity increases starting from rest. However, Hu *et al.* (2000) calculated the protein concentration distribution across the glycocalyx layer and found that the concentration drops sharply across the ESL and that the layer serves as a molecular sieve. This view is strongly supported by the recent experiments of Adamson *et al.* (2004) where the oncotic forces across the ESL are measured. Loss of this molecular sieve by hyaluronidase treatment (Van den Berg, Vink & Spaan 2003) results in subendothelial edema formation, consistent with the associated loss of protein concentration drop across the glycocalyx. Thus, the oncotic pressure of the adsorbed proteins of the blood plasma would have to exceed the oncotic pressure induced by the ESL as a molecular sieve for oncotic swelling of the ESL to occur.

Vink, Wieringa & Spaan (1995) showed that repulsion of negative charges on the membrane of red blood cells by anionic glycocalyx sites influences capillary

FIGURE 7. The time-dependent change in shape of the core protein fibre (*a*) and the normal (*b*) and tangential (*c*) components of its local hydrodynamic loading during ESL restoration after the passage of a WBC. The dotted lines in (*b*) show the hydrodynamic loading on the flat portion of the core protein fibre, which is balanced by the restoring force of the fibres in the matted layer beneath it.

hemodynamics, and Vink & Duling (2000) found that negatively charged molecules diffuse more slowly into the glycocalyx than their neutral counterparts. Stace and Damiano (2001) proposed that this is due to fixed negative charges that are bound to the glycocalyx fibres. They modelled the glycocalyx layer as a diffusely distributed anionic mucopolysascharide matrix without an elastic restoring capability. Based on this picture of the glycocalyx layer, they developed a mechano-electrochemical model to predict the recovery time of the glycocalyx layer after its compression by the passage of a WBC (Damiano & Stace 2002). The fundamental premise is that mechanical deformations of the layer caused by the passage of the WBC produce a departure from a near electroneutral equilibrium. This creates gradients of electrochemical potential that result in a redistribution of mobile ions and a rehydration of the layer after its compression. The model can predict recovery times that agree with experiment and restoration profiles that are similar to this study, see figure 6, provided the ratios of glycocalyx fixed charge concentration to mobile ion concentration and the cationic charge density of blood are chosen to provide an optimum two-parameter fit.

The third hypothesis, proposed by Weinbaum *et al.* (2003), is that the core proteins in the ESL depicted in figure 1 have a finite flexural rigidity sufficient to withstand significant deformations of the glycocalyx layer due to blood flow and large enough to restore the layer after a large-amplitude compression by passing WBCs. Important experimental evidence in support of this hypothesis is the fact that the quasi-periodic structure for the distribution of the molecular level scattering centres along the axes of the core proteins observed in Squire *et al.* (2001) would not be possible in the presence of thermal fluctuations due to Brownian motion unless the core proteins had a non-negligible flexural rigidity. To this end the model in Weinbaum *et al.* (2003) predicts that the value of EI, 700 pN nm^2, required to restore the ESL after the passage of a WBC is also sufficient to limit deflections of the core proteins to at most a few percent of their length at physiological flow rates.

The elastic model in Weinbaum *et al.* (2003) provides only a reasonable characteristic time for the restoration of the compressed glycocalyx layer. It is too simplified to provide realistic predictions for the time-dependent changes in shape of the core proteins or detailed predictions of the recovery profiles for ESL thickness that can be compared with the experimentally measured restoration curves in figure 3. The theory for small deflections in Weinbaum *et al.* (2003) describes only the final approach to equilibrium, neglects the y component of the velocity and treats the fluid in the matrix layer as a stagnant fluid. The present model for large fibre deformations is superior in that it corrects all of these shortcomings and also considers in an approximate manner the difficulties that arise from an ESL with overlapping fibres at its edge for large compressions. This is clearly illustrated in figure 6 where the theory provides good agreement with experiment for both phase I and phase II of the restoration process using only a single curve-fitting parameter EI.

The oncotic (Secomb *et al.* 2001*a*, *b*), the mechano-electrochemical (Damiano & Stace 2002; Stace & Damiano 2001) and the elastic (Weinbaum *et al.* 2003) theoretical models all agree that the flow within the glycocalyx layer is negligible and that this layer shields the endothelial cell membrane from the direct shearing of the blood flow. Thus, these models also need to address the issue of mechanotransduction across the glycocalyx layer in addition to the mechanical properties that provide its stiffness. Both the 'oncotic force' and the 'mechano-eletrochemical' models neglect the flexural rigidity of the core proteins and assume that the fluid shear stress is passively transmitted to the membrane of endothelial cells as a surface traction. The basic question is how the fluid shear is transmitted across the endothelial membrane to

the actin cortical web. In the oncotic force model a tangential component of tension develops along the ESL fibres due to fluid shear and is transmitted as a traction force to the intracellular cytoskeleton via the transmembrane proteins that form the attachment points for the ESL fibres. In the elastic model described herein fluid shear induces bending moments on the ESL fibres due to their finite flexural rigidity. These fibres are assumed to be rigidly linked by transmembrane proteins to the stiffer actin cortical cytoskeleton beneath the membrane.

The recent experiments of Thi *et al.* (2004) show that in the presence of plasma proteins, either 1% bovine serum albumin or fetal bovine serum, there was a reorganization of the actin cytoskeleton and a redistribution of associated linker molecules, such as vinculin, in rat fat pad endothelial cells in response to a fluid shear of 10 dyn cm^{-2} for 5 h. This response could be completely abolished at the same fluid shear stress applied for the same duration if the plasma proteins were removed or the ESL was enzymatically treated with heparinase. In either case more than half the ESL fibres were still present, but they were unable to transmit the tangential stress across the membrane and there was no cytoskeletetal reorganization. Thi *et al.* explain this behaviour in terms of the elastic model described herein. In this model the bending moment on the actin cytoskeleton is transmitted to the dense peripheral actin band associated with the adherens junction at the border of the cell. This model predicts that at a shear stress of 10 dyn cm^{-2} the integrated bending moment on the adherens junction is sufficient to 'unzip' the VE-cadherin linkage between adjacent cells and initiate a disruption of the dense peripheral actin bands.

This study has been supported by National Heart, Lung, and Blood Institute Grant HL-44485, the Netherlands Organization for Scientific Research (grant # 902-16-192 and # 902-16-205), a fellowship to Hans Vink from the Royal Netherlands Academy of Arts and Sciences (KNAW), and was performed in partial fulfillment of the requirements for the PhD degree of Y. Han from CUNY.

REFERENCES

Adamson, R. H., Lenz, J. F., Zhang, X., Adamson, G. N., Weinbaum, S. & Curry, F. E. 2004 Oncotic pressures opposing filtration across non-fenestrated rat microvessels. *J. Physiol.* **557**, 889–907.

Blake, J. R. 1971 A spherical envelope approach to ciliary propulsion. *J. Fluid Mech.* **46**, 199–208.

Constantinescu, A. A., Vink, H. & Spaan, J. A. 2001 Elevated capillary tube hematocrit reflects degradation of endothelial cell glycocalyx by oxidized LDL. *Am. J. Physiol. Heart Circ. Physiol.* **280**, H1051–H1057.

Cowin, S. C., Weinbaum, S. & Zeng, Y. 1995 A case for bone canaliculi as the anatomical site of strain generated potentials. *J. Biomechanics*, **28**, 1281–1297.

Damiano, E. R. 1998 The effect of the endothelial-cell glycocalyx on the motion of red blood cells through capillaries. *Microvasc. Res.* **55**, 77–91.

Damiano, E. R., Duling, B. R., Ley, K. & Skalak, T. C. 1996 Axisymmetric pressure-driven flow of rigid pellets through a cylindrical tube lined with a deformable porous wall layer. *J. Fluid Mech.* **314**, 163–189.

Damiano, E. R. & Stace, T. M. 2002 A mechano-electrochemical model of radial deformation of the capillary glycocalyx. *Biophys. J.* **82**, 1153–1175.

Dupuis, D. E., Guilford, W. H., Wu, J. & Warshaw, D. M. 1997 Actin filament mechanics in the laser trap. *J. Muscle Res. Cell Motil.* **18**, 17–30.

Feng, J., Ganatos, P. & Weinbaum, S. 1998 Motion of a sphere near planar confining boundaries in a Brinkman medium. *J. Fluid Mech.* **375**, 265–296.

Feng, J. & Weinbaum, S. 2000 Lubrication theory in highly compressible porous media: the mechanics of skiing, from red cells to humans. *J. Fluid Mech.* **422**, 281–317.

Frisch-Fay, R. 1962 *Flexible Bars*. Washington, Butterworths.

Gere, J. M. & Timoshenko, S. P. 1990 *Mechanics of Material*. Boston, PWS-KENT Publishing Company.

Gittes, F., Mickey, B., Nettleton, J. & Howard, J. 1993 Flexural rigidity of microtubules and actin filaments measured from thermal fluctuations in shape. *J. Cell Biol.* **120**, 923–934.

Guo, P., Weinstein, A. M. & Weinbaum, S. 2000 A hydrodynamic mechanosensory hypothesis for brush border microvilli. *Am. J. Physiol. Renal. Physiol.* **279**, F698–F712.

Han, Y., Ganatos, P. & Weinbaum, S. 2005 Transmission of steady and oscillatory fluid shear stress across epithelial and endothelial surface layers. *Phys. Fluids* **17**, 031508(1–13).

Henry, C. B. & Duling, B. R. 2000 TNF-alpha increases entry of macromolecules into luminal endothelial cell glycocalyx. *Am. J. Physiol. Heart Circ. Physiol.* **279**, H2815–H2823.

Hu, X., Adamson, R. H., Liu, B., Curry, F. E. & Weinbaum, S. 2000 Starling forces that oppose filtration after tissue oncotic pressure is increased. *Am. J. Physiol. Heart Circ. Physiol.* **279**, H1724–H1736.

Lee, B. K., Wilson, J. F. & Oh, S. J. 1993 Elastica of cantilevered beams with variable cross sections. *Intl J. Non-linear Mech.* **28**, 579–589.

Liron, N. & Mochon, S. 1976 Stokes flow for a Stokeslet between two parallel flat plates. *J. Engng. Maths* **10**, 287–303.

Liron, N. & Shahar, R. 1978 Stokes flow due to a Stokeslet in a pipe. *J. Fluid Mech.* **162**, 157–170.

Liu, W., Xu, S., Woda, C., Kim, P., Weinbaum, S. & Satlin, L. M. 2003 Effect of flow and stretch on the $(Ca^{2+})_i$ response of principal and intercalated cells in cortical collecting duct. *Am. J. Physiol. Renal Physiol.* **285**, F998–F1012.

Michel, C. C. 1997 Starling: the formulation of his hypothesis of microvascular fluid exchange and its significance after 100 years. *Expl Physiol.* **82**, 1–30.

Mulivor, A. W. & Lipowsky, H. H. 2004 Inflammation- and ischemia-induced shedding of venular glycocalyx. *Am. J. Physiol. Heart Circ. Physiol.* **286**, H1672–H1680.

Pries, A. R., Secomb, T. W. & Gaehtgens, P. 2000 The endothelial surface layer. *Pflugers. Arch.* **440**, 653–666.

Pries, A. R., Secomb, T. W., Jacobs, H., Sperandio & Gaehtgens, P. 1998 Blood flow resistance during hemodilution: effect of plasma composition. *Cardiovasc. Res.* **37**, 225–235.

Pries, A. R., Secomb, T. W., Jacobs, H., Sperandio, M., Osterloh, K. & Gaehtgens, P. 1997 Microvascular blood flow resistance: role of endothelial surface layer. *Am. J. Physiol.* **273**, H2272–H2279.

Sangani, A. S. & Acrivos, A. 1982 Slow flow past periodic arrays of cylinders with application to heat transfer. *Int. J. Multiphase Flow* **8**, 193–206.

Secomb, T. W., Hsu, R. & Pries, A. R. 1998 A model for red blood cell motion in glycocalyx-lined capillaries. *Am. J. Physiol.* **274**, H1016–H1022.

Secomb, T. W., Hsu, R. & Pries, A. R. 2001*a* Effect of the endothelial surface layer on transmission of fluid shear stress to endothelial cells. *Biorheology* **38**, 143–150.

Secomb, T. W., Hsu, R. & Pries, A. R. 2001*b* Motion of red blood cells in a capillary with an endothelial surface layer: effect of flow velocity. *Am. J. Physiol. Heart Circ. Physiol.* **281**, H629–H636.

Squire, J. M., Chew, M., Nneji, G., Neal, C., Barry, J. & Michel, C. 2001 Quasi-periodic substructure in the microvessel endothelial glycocalyx: a possible explanation for molecular filtering? *J. Struct. Biol.* **136**, 239–255.

Stace, T. M. & Damiano, E. R. 2001 An electrochemical model of the transport of charged molecules through the capillary glycocalyx. *Biophys. J.* **80**, 1670–1690.

Sugihara-Seki, M. 2005 A fluid-mechanical study for solute transport across the endothelial surface glycocalyx. *2005 Summer Bioengineering Conference of the ASME Bioengineering Division, Vail, CO, USA, June 22–26.*

Thi, M. M., Tarbell, J. M., Weinbaum, S. & Spray, D. C. 2004 The role of the glycocalyx in reorganization of the actin cytoskeleton under fluid shear stress: A "bumper-car" model. *Proc. Natl Acad. Sci. USA* **101**, 16483–16488.

Van den Berg, B. M., Vink, H. & Spaan, J. A. E. 2003 The endothelial glycocalyx protects against myocardial edema. *Circ. Res.* **92**, 592–594.

Vink, H., Constantinescu, A. A. H. & Spaan, J. A. E. 2000 Oxidized lipoproteins degrade the endothelial surface layer: implications for platelet-endothelial cell adhesion. *Circulation* **101**, 1500–1502.

Vink, H. & Duling, B. R. 1996 Identification of distinct luminal domains for macromolecules, erythrocytes, and leukocytes within mammalian capillaries. *Circ. Res.* **79**, 581–589.

Vink, H. & Duling, B. R. 2000 Capillary endothelial surface layer selectively reduces plasma solute distribution volume. *Am. J. Physiol. Heart Circ. Physiol.* **278**, H285–H289.

Vink, H., Duling, B. R. & Spaan, J. A. E. 1999 Mechanical properties of the endothelial surface layer (Abstract). *FASEB J.* **13**, A11.

Vink, H., Wieringa, P. A. & Spaan, J. A. E. 1995 Evidence that cell surface charge reduction modifies capillary red cell velocity-flux relationships in hamster cremaster muscle. *J. Physiol.* **489.1**, 193–201.

Weinbaum, S. 1998 1997 Whitaker Distinguished Lecture: Models to solve mysteries in biomechanics at the cellular level; a new view of fibre matrix layers. *Ann. Biomed. Engng* **26**, 627–643.

Weinbaum, S., Zhang, X., Han, Y., Vink, H. & Cowin, S. C. 2003 Mechanotransduction and flow across the endothelial glycocalyx. *Proc. Natl Acad. Sci. USA* **100**, 7988–7995.

Wiederhielm, C. A. & Black, L. L. 1976 Osmotic interaction of plasma proteins with interstitial macromolecules. *Am. J. Physiol.* **231**, 638–641.